Journal of
Intelligent Material
Systems and Structures

Article

Journal of Intelligent Material Systems and Structures
24(8) 973–983

DOI: 10.1177/1045389X12461074
jim.sagepub.com
SAGE

Radio frequency patch antenna reconfiguration with Ni–Ti shape memory alloy switches

Paul J Wolcott[1], Zheyu Wang[2], Lanlin Zhang[2] and Marcelo J Dapino[1]

Abstract

Nickel–titanium shape memory alloys are employed to develop a multiband radio frequency antenna. Switches made from Ni–Ti electronically connect together a planar patch antenna arrangement, creating several electrical signal pathways that enable reconfiguration via resonance shifting. The changes in the antenna geometry, induced by the switches, create different working frequencies. The switches open and close due to an induced phase change from martensite to austenite via resistive heating from a separate electric circuit. A patch antenna was fabricated and then measured for S_{11} reflection coefficient, antenna gain, and radiation pattern at different configurations. The results show that the working frequency of the patch antenna arrangement is tunable from 2.25 to 2.43 GHz depending on the antenna geometry, while the antenna always maintains a high gain. The experimental results match well with simulations, indicating the potential for simulated design of future applications and geometries through shape memory actuators.

Keywords

Shape memory alloys, radio frequency antennas, patch antenna, Ni–Ti

Introduction

Small, multifunctional radio frequency (RF) devices are critical in commercial and military communications. Examples of their use include portable devices for high data rate communications via ground and satellite means; miniature ultra wideband antennas on thin, flexible substrates in unmanned aerial vehicles (UAVs); multifunctional/reconfigurable apertures; and many more. These applications are of growing importance and the need to develop improved devices for such applications is essential.

Many antenna types and geometries can be considered to achieve multifunctional performance for portable devices. The microstrip, or patch antenna type, is unique in that it is low profile, lightweight, compact, and conformable to a mounting structure as compared to other antenna types (Balanis, 2008). These factors, in addition to a low observability, have made patch antennas desirable in a number of military and commercial applications in aerospace and mobile satellite communications. Despite the advantages this antenna type provides, its use has been limited due to its narrow bandwidth (Targonski et al., 1998). The narrow bandwidth limits the versatility of the antenna, making it impractical for many modern communication applications (Yang and Luk, 2006). Achieving frequency reconfiguration can overcome this disadvantage, allowing for more prevalent use of patch antennas in advanced applications.

Patch antennas consist of a ground plane, substrate, radiation aperture, and coaxial connector. A typical patch antenna layout is shown in Figure 1. The radiation aperture geometry dictates most of the RF performance of the antenna (Balanis, 2008). Like other antenna types, the patch antenna is usually operated at resonance. In this case, the effective electrical length of the patch radiator governs the operating frequency, bandwidth, and radiation pattern of the antenna (Bernhard, 2007). Since the effective electrical length of an antenna is a function of geometry, capacitance, and dielectric constant, the antenna's resonance frequency

[1]Smart Materials and Structures Laboratory, Department of Mechanical and Aerospace Engineering, The Ohio State University, Columbus, OH, USA
[2]ElectroScience Laboratory, Department of Electrical and Computer Engineering, The Ohio State University, Columbus, OH, USA

Corresponding author:
Marcelo J Dapino, Smart Materials and Structures Laboratory, Department of Mechanical and Aerospace Engineering, The Ohio State University, 201 West 19th Avenue, Columbus, OH 43210, USA.
Email: dapino.1@osu.edu

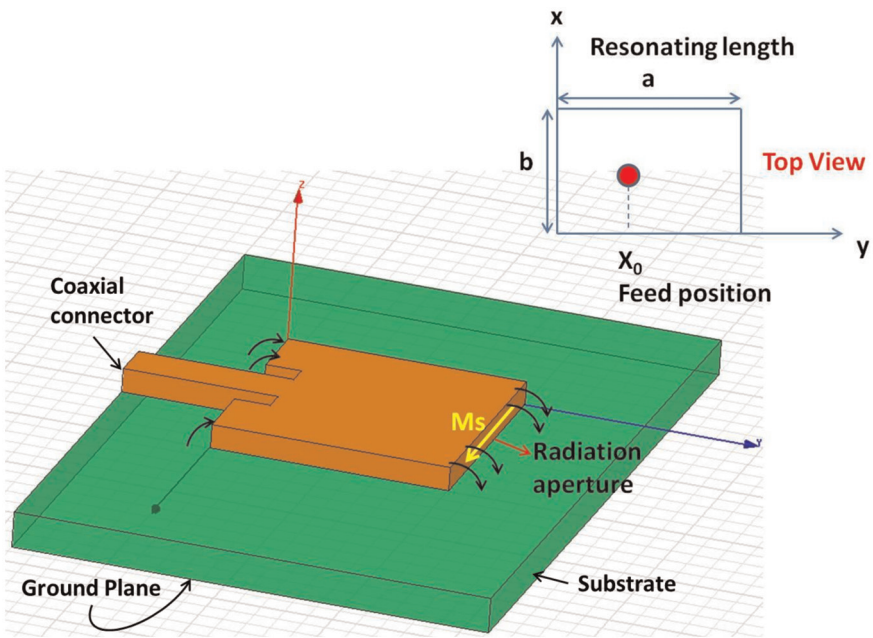

Figure 1. Example patch antenna with geometry used in prototype patch antenna model.

can be tuned by controlling these properties (Ghosh and Parui, 2010).

Changes in antenna electrical properties such as capacitance or dielectric constant create controllable, solid-state variations in the electrical properties of the component materials to achieve variable operating frequencies (Yashchyshyn, 2010). Varactor diodes have been used to control capacitance and tune an antenna's natural frequency. In this design, each diode has a capacitance controlled by its biased voltage, and these capacitances alter the effective permittivity of the substrate and therefore its resonant frequency (Lee, 1989). This design has been successful in tuning the frequency of microstrip antennas over a 20%–30% band range with the advantage that the frequency can be tuned continuously (Bhartia and Bahl, 1982). However, because the diodes need to be placed at the edges of the antenna, a limited range of geometries can be implemented in practice.

Geometric changes are often achieved through switching mechanisms that change the signal pathway of the patch radiator to change the operating frequency. In this case, creating a larger geometry lowers the effective natural frequency while smaller geometries increase the natural frequency. This type of reconfiguration has the advantage of allowing more complex antenna geometries to be realized. Recent work has focused on the use of Micro-Electro-Mechanical Systems (MEMS) devices as switches to alter the geometry of the antenna to tune frequency (Anagnostou et al., 2006). In this type of design, sets of MEMS switches controllably connect to an antenna to change the effective geometry by making it larger or smaller depending on the switch configuration on the antenna (Vinoy and Varadan, 2001). MEMS devices provide a low-powered, isolated method of antenna reconfiguration but cannot provide the large-scale frequency shifts possible in mechanical reconfiguration due to their size (Bernhard, 2007). Mechanical reconfiguration through dimensional changes is a robust method of creating large natural frequency shifts in the antenna with a comparably low number of switches. This reconfiguration can be achieved with a number of methods, such as the electrostatic actuator application in Bernhard et al. (2001). This design shows promise, although it is far too bulky to be considered viable in many applications.

Other geometric methods, such as using smart material switches made from shape memory alloys (SMAs), provide a compact, robust method to create large changes in the operating frequency without significant degradation in the antenna performance. This method has been tested and verified using monopole and microstrip line geometries and requires further investigation when applied to planar geometries (Wolcott et al., 2011).

SMAs are promising for antenna reconfiguration. In these alloys, thermomechanical transformation between martensitic and austenitic phases produces strain recovery with heating (Lagoudas, 2008). Using the shape memory effect, a trained shape can be developed that can be recovered with heat (Kai and Chengin, 2002). The martensitic phase is a monoclinic structure that can have a twinned or detwinned form. Stress acting on the twinned state rearranges the alternating monoclinic orientations in one direction to form the detwinned phase. Heating causes a solid-state phase change to

austenite, a cubic crystalline microstructure. Upon cooling, the microstructure returns to the twinned martensite phase when no stress is applied to the material (Otsuka and Wayman, 1999).

Equiatomic nickel–titanium (Ni–Ti) can recover up to 6% strain when heated above its austenitic finish temperature (Davis, 2003). The high deformation and stiffness provided by these materials allow for high-density, solid-state actuators to replace massive and bulky actuators based on conventional technologies (Kim et al., 2011; Liang and Rogers, 1997). One type of Ni–Ti actuator is the bias force actuator. This type of actuator uses a bias spring to generate the restoring force in the one-way shape memory effect (Liang and Rogers, 1997). The Ni–Ti actuator begins in the deformed state at low temperature and when heated deflects a spring that stores the potential energy. When the Ni–Ti element is cooled, the potential energy stored in the spring is released and deforms the material to its original position (Liang and Rogers, 1997). This type of actuator can utilize an elastic beam as the spring to restore the deformed position, as is performed in this study.

A key disadvantage of using SMAs for reconfiguration is the slow switching speed. Although this can be mitigated to a degree by increasing the current to accelerate heating, using forced air to speed cooling or by miniaturizing the switches to increase heat transfer, there will always be limitations based on the actuation speed. It is therefore emphasized that SMAs for reconfiguration are more practical in communication applications where microsecond-order switching is not necessary.

This study investigates the implementation of Ni–Ti switches in a radiating, planar patch antenna building upon the principles presented in Wolcott et al. (2011) to create a robust, reconfigurable front end antenna. The switches use design elements of a bias spring type actuator using an elastic beam as the bias spring. The SMA actuators provide a switching mechanism to create a change in the geometry of the antenna and an associated shift in the working frequency.

SMA switch design

Two normally open switches were built using the principles outlined in Wolcott et al. (2011). The design for each switch uses a Ni–Ti ribbon on top of a spring steel beam, electrically insulated from one another with Kapton tape. A side view schematic of the switch design and motion is shown in Figure 2. The Ni–Ti strip begins in the detwinned martensite phase when the switch is off. The Ni–Ti ribbon is split in the center, as shown in Figure 3, to create an electric circuit for current to resistively heat the Ni–Ti strip. A 2.75-A direct current (DC) is applied to heat the strip and transform it into the trained austenite phase. As the heating and

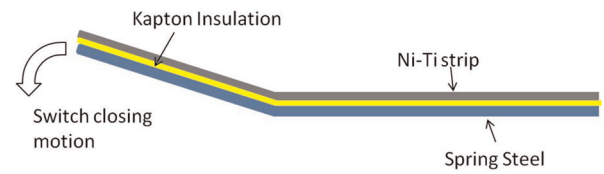

Figure 2. Schematic representation of switch components and motion.

Figure 3. Schematic of Ni–Ti strip circuit for resistive heating.

transformation occur, the Ni–Ti strip pushes down the spring steel until an electrical contact is made with the patch antenna. When the current is turned off, the Ni–Ti strip cools and the spring steel deforms the Ni–Ti strip upward, returning to the detwinned switch off state. The split tails of the Ni–Ti strip are fixed onto the antenna and connected to a power supply while the actuation side of the switch is free to move up and down to connect and disconnect with the main patch. This design is a normally open configuration because when no current is supplied to the Ni–Ti strip, there is no electrical contact with the patch antenna causing reconfiguration. A normally closed design can be implemented in analogous manner.

Figure 4 shows an image of the two switches, labeled A and B. As shown in Table 1, the overall dimensions of the switches are slightly larger than the sum of the Ni–Ti strip and spring steel due to the Kapton insulation. The two switches are similarly sized, making it easier to implement them symmetrically into the antenna design. The transformation temperatures of the Ni–Ti strip used in both switches were measured with differential scanning calorimetry and were found to be: A_s = 58°C, A_f = 71°C, M_s = 51°C, and M_f = 42°C. A_s is the austenite start temperature where the Ni–Ti strip begins its phase change to austenite upon heating. Here, A_f is the austenite finish temperature representing the temperature when the Ni–Ti strip is fully transformed to austenite; M_s is the martensite start temperature where the Ni–Ti strip begins its transition back to the martensite phase upon cooling; and M_f is the martensite finish temperature representing the temperature when the Ni–Ti strip has fully transformed back to the martensite phase.

SMA switch testing

To evaluate the SMA switch actuation, tests were conducted on each switch to ensure they were opening and closing properly. These tests consisted of actuating each

Table 1. Switch dimensions (overall dimensions include Kapton insulation).

	Switch A			Switch B		
	Length (mm)	Width (mm)	Thickness (mm)	Length (mm)	Width (mm)	Thickness (mm)
Ni–Ti	33.8	3.5	0.254	33.5	3.5	0.254
Spring steel	22.2	3.5	0.127	35.5	5.3	0.127
Overall	33.8	5.6	0.762	36.1	6.8	0.762

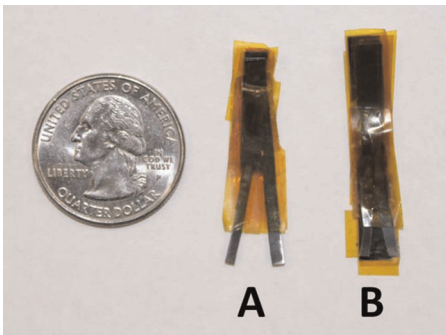

Figure 4. Image of the two antenna switches, labeled A and B.

switch separately via power supply at 2.75 A and measuring the time it took to close and open a contact between two copper wires. The copper wires were connected to a separate power supply, producing approximately 0.5 A current. Copper tape was placed on the actuating tip of the SMA switches for electrical conduction, and the current in each circuit was measured. Once contact was made between the switch and the copper wires, the resistive heating of the SMA was turned off, and the time for the switch to actuate upward, breaking the circuit, was measured.

The opening and closing of the contact for Switch A takes approximately 8 s while Switch B closes contact in approximately 8 s and opens the circuit in approximately 15 s. The differences in actuation between the two switches are attributed to the slight differences in their geometries. The actuation time can be optimized by altering the current used for heating or by supplying air to remove heat more quickly. The removal of heat is the rate-limiting step with these switches, as with most SMAs, and therefore increasing the airflow rate from zero would increase cooling by convection to minimize actuation time. Likewise, further miniaturization of the switches would decrease switching time, but since the focus of this study is on proving reconfiguration in a planar device, these methods were not pursued. Based on these tests, the switch actuation for each SMA switch is confirmed as working properly.

Patch antenna design

The initial design of the reconfigurable patch antenna consisted of a rectangular prototype patch antenna model with dimensions $a \times b$ in the $x-y$ plane, with $a > b$ as shown in Figure 1. From Balanis (2005), a cavity model was used to analyze the antenna radiation for this prototype design. The wave equation for the patch cavity is

$$\nabla^2 \vec{E_z} + k^2 \vec{E_z} = -j\omega\mu \vec{J_z}$$
$$\vec{E_z} = \sum_{m=0}^{\infty}\sum_{n=0}^{\infty} C_{nm} \cos\frac{n\pi y}{a}\cos\frac{m\pi x}{b} \tag{1}$$

where J_z is the input current, E_z is the electric field in the $x-y$ plane of the cavity, k is the propagation constant, ω is the frequency, and μ is the permeability of the substrate. The patch antenna is considered to be a dielectric-loaded cavity having two perfectly conducting electric walls (top and bottom) and four perfectly conducting magnetic walls (sidewalls). Antenna radiation takes place at the four sidewalls (radiation apertures). Using the field equivalence principle, the equivalent magnetic current density, M_s, is obtained at the four apertures as

$$M_s = -2 \cdot \hat{n} \times E_{aperture} \tag{2}$$

where $E_{aperture}$ is the electric field (E_z) on the aperture. The far-zone electric field radiated by each aperture is calculated using the equivalent current density

$$\vec{E} = \frac{\mu}{4\pi}\int_{-\frac{b}{2}}^{\frac{b}{2}}\int_{-\frac{a}{2}}^{\frac{a}{2}} M_s \frac{e^{-jkr}}{r}\,dxdy. \tag{3}$$

Here, r is the distance between the observation point in the far field and the radiation origin. The antenna's natural frequency is mainly determined by the resonating length of the patch (Arcioni et al., 2007; Balanis, 2005). Therefore, the patch antenna can be reconfigured by incorporating capacitive switches to modify the patch length a, in this case through SMA switches.

As represented in Figure 5, the reconfigurable design consists of a main patch element (54.0 mm × 40.0 mm) with two unattached strips (21.3 mm × 1.0 mm). Because there are two unattached segments, there are four possible geometries: (a) neither switch connected, (b) Switch A on and Switch B off, (c) Switch A off and Switch B on, and (d) both switches on. The feed and

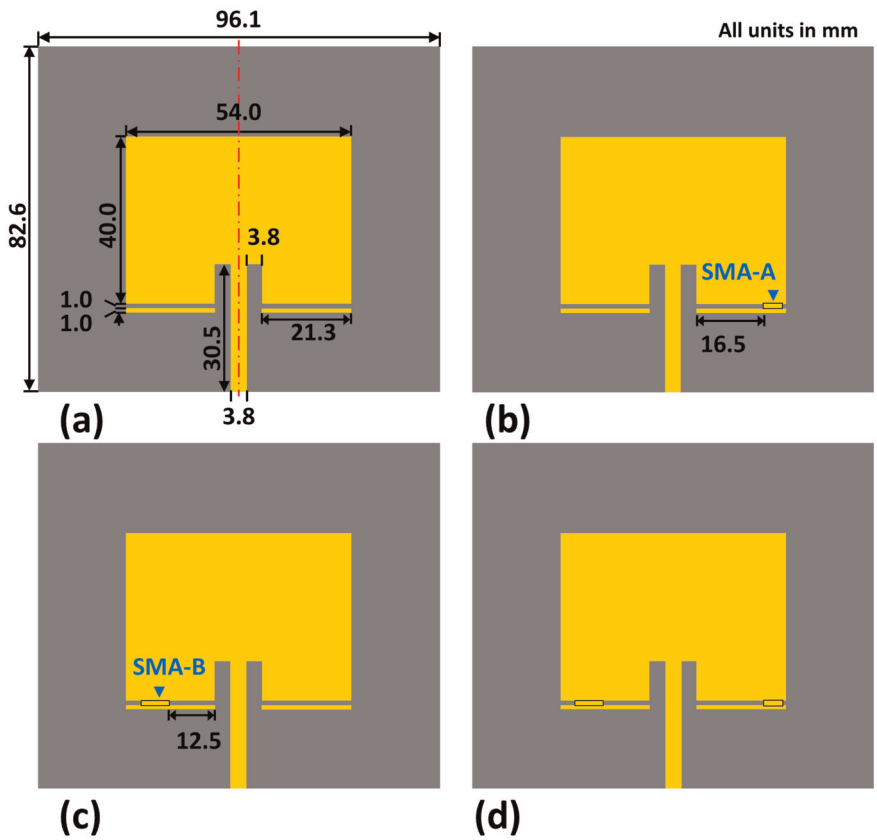

Figure 5. Reconfigurable patch antenna dimensions at the four corresponding geometries: (a) both switches off, (b) Switch A on and Switch B off, (c) Switch A off and Switch B on, and (d) both switches on.
SMA: shape memory alloy.

switch locations were chosen to achieve an optimal impedance match. For this design, the switches are placed on the antenna such that in the on state, the switches mechanically deform and contact the two unattached segments below the main patch antenna. Electrical connection is then established between the segments and the patch, resulting in an effective increase in the antenna dimensions and reconfiguration to be realized. As a result, compared to the off state, the antenna is reconfigured to have effectively larger dimensions, exhibiting a correspondingly lower characteristic resonance frequency.

Antenna performance simulation results

Ansoft HFSS three-dimensional full-wave electromagnetic (EM) field simulation software was employed to analyze the antenna's reflection coefficient and radiation characteristics at the various switch configurations. Figure 6 presents the simulated antenna performance for a number of parameters at the various geometries, while Figure 7 provides the varied surface current distribution at different switch configurations. For these simulations, an ideal electrical contact was assumed between the strips and the main patch in the on state. Parameter S_{11} represents the reflection coefficient of the antenna, indicating the amount of power lost at the input port (Pozar, 2008). The operating resonant frequency of an antenna is determined where minimum reflection (minimum S_{11}) occurs.

Antenna gain represents the quantity and frequency of EM waves transmitted in a specific direction and is defined as the ratio of radiation intensity in a given direction to the radiation intensity of a reference antenna (Balanis, 2005). The gain is useful in determining the operating efficiency of an antenna, where higher values represent efficient power transmittance and its operating frequency. The radiation pattern of an antenna is the spatial distribution of transmitted power from the antenna signal (Balanis, 2005). In this case, the value is given as a normalized value of the peak gain varying with the degree of rotation from normal. The pattern indicates the direction in which the antenna most efficiently transmits EM power and therefore is useful in maximizing transmittance in the desired directions. In this case, with a planar antenna, it is expected that most of the pattern will be oriented normal (0°) to the antenna surface.

From the results of the simulation, a clear shift in the frequency of S_{11} and gain is shown between

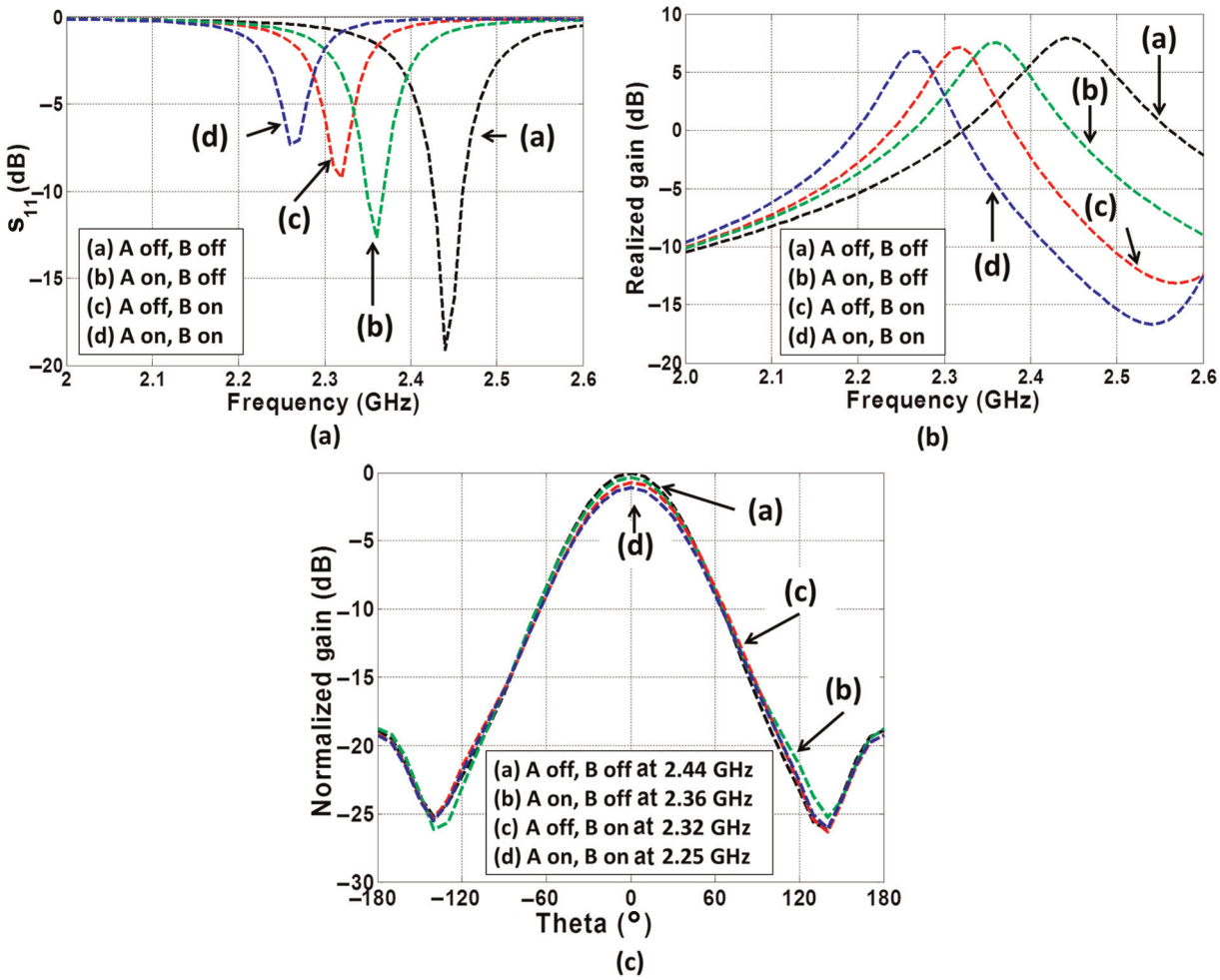

Figure 6. Simulation results for (a) S_{11} signal reflection, (b) antenna gain, and (c) radiation pattern.

different geometries. The resonance frequency shifts from 2.44 GHz with no switches activated to 2.27 GHz with both switches activated. The difference in response between the switch-on geometries is due to the asymmetry in the reconfigurable patch design. The increase in S_{11} and decrease in gain is caused by the geometry changes causing an impedance mismatch; it is emphasized that the impedance was matched for the original system with both switches in the off state. Due to the changes in geometry it is expected that a small decrease in performance will exist due to the impedance changing with geometry. At least 6-dB gain is achieved in all configurations, which is important for efficient high-performance wireless communications. As expected, the shift in frequency shown in the S_{11} results is consistent with the gain results.

The radiation pattern is consistent between each of the configurations as is expected from the design. Although an asymmetry exists in the switch geometries, it is not significant enough to alter the radiation pattern. Pattern reconfigurability is another area of work that has been demonstrated in the literature (Kim et al., 2011); however, the focus of this work is frequency reconfiguration and therefore pattern reconfiguration was limited in the design of this device. Additionally, it is seen in Figure 7 that in the on states, the increase in resonating length caused by the switches causes shifts in the antenna surface current distribution. This is the expected result of the reconfiguration causing a shift in the electrical pathway of the patch radiator element.

Antenna construction and switch implementation

Following the simulation, the reconfigurable patch antenna with SMA switches was fabricated. The antenna pattern was fabricated by laser milling a copper layer cladded onto a Duroid 5880 dielectric substrate (ε_r = 2.2, tan δ = 0.0009, thickness = 1.575 mm) with a copper ground plane. Figure 8 shows a schematic side view of the fabricated antenna with one SMA switch for reconfiguration. Copper tapes were placed on the actuating end of the switches to provide electrical contact between the antenna and the activated switches.

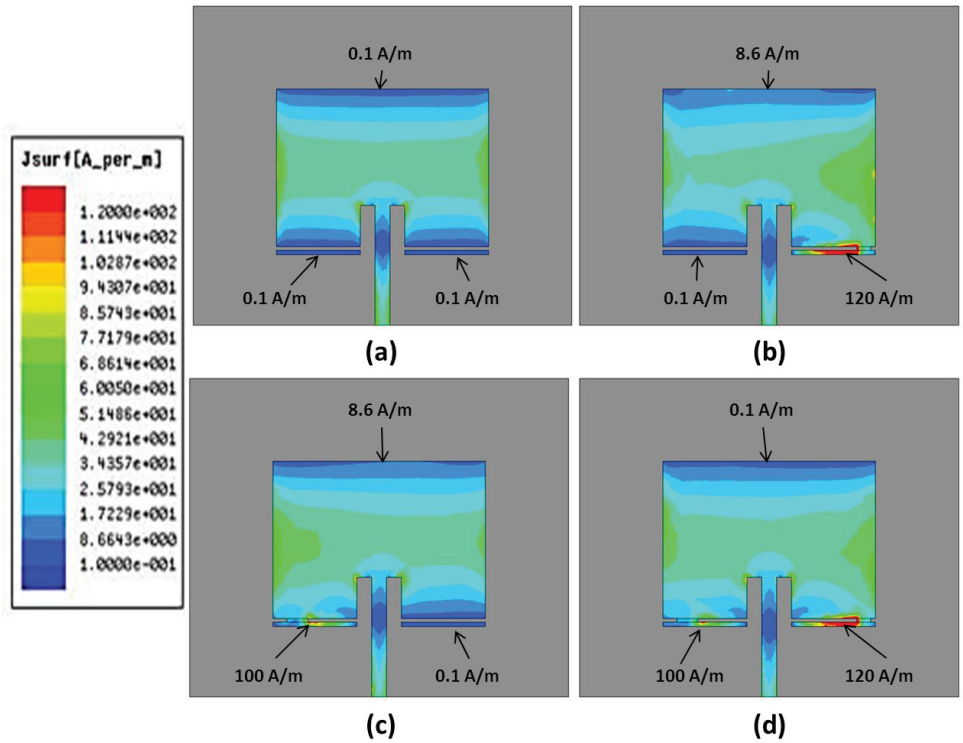

Figure 7. Surface current distribution (range: 0.1–120 A/m) on patch antenna at four corresponding geometries: (a) both switches off, (b) Switch A on and Switch B off, (c) Switch A off and Switch B on, and (d) both switches on.

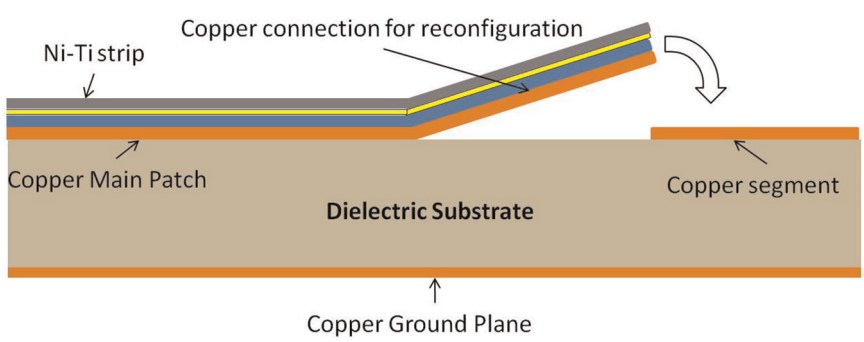

Figure 8. Side view schematic of switch mechanism opening and closing for reconfiguration.

The four reconfiguration geometries used for testing are shown in Figure 9 with switches attached or unattached to show the representative antenna shapes. During operation, all switches are attached to the antenna and are controllably heated to close the electrical circuit to realize the different geometries.

Antenna testing

To validate the antenna reconfiguration, the S_{11} reflection coefficient, realized gain, and radiation pattern were measured for all four antenna configurations. All four configurations are shown in Figure 9 and are the same as the simulation. The tail portion of the switches was fixed onto the main patch antenna, while the actuating end of the switches connected the segment to the main patch when activated.

The S_{11} reflection coefficient was measured using a network analyzer (Agilent N5242A, PNA-X) over the frequency range from 1 to 6 GHz. As shown in Figure 10(a), the resonance frequency was 2.43 GHz with both switches off. This configuration provided a baseline for antenna performance when no reconfiguration was attempted. When only Switch A or B was on, only one segment was connected to the main antenna. This creates larger antenna dimensions and a lower resonance occurred at 2.32 or 2.31 GHz, respectively. The difference between the resonance frequencies was attributed to the slight difference in dimensions between Switch A and Switch B. Finally, when both switches were on,

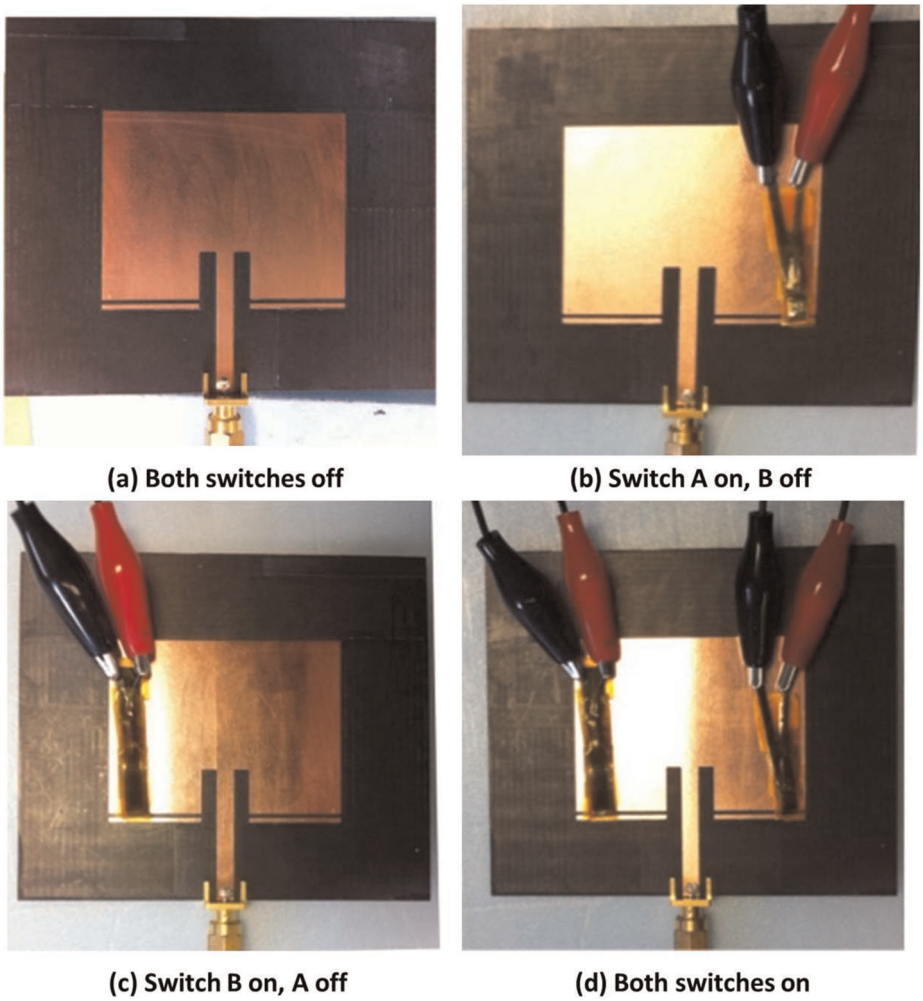

Figure 9. Antenna geometries for the switches in on and off states.

both segments were connected to the antenna. The effective antenna size further increased and the resonance shifted to 2.25 GHz. The maximum frequency shift from both switches on to both switches off was 180 MHz. It is noted that the S_{11} of all four configurations was lower than or close to -10 dB. This indicates that the reflected power was less than or close to 10%, which is satisfactory for a working antenna. The increases in S_{11} for the switch on geometries are attributed to an impedance mismatch between the switches and the antenna patch in the reconfigured geometries.

Measurements of the realized gain and radiation patterns were performed subsequently in an anechoic chamber (chamber with acoustic foam used to eliminate EM reflections and outside RF noise). As shown in Figure 10(b), each activated geometry exhibited a high gain (>5 dB) and shift in resonance frequency. As in the other tests, the slightly lower gain compared to the simulation was due to a slight impedance mismatch in these geometries. The radiation pattern (Figure 10(c)) confirmed the antenna directionality at the resonance frequency for each configuration, in agreement with the characteristics of patch antennas. These results validate the effectiveness and high-gain performance of the reconfigurable antenna.

Comparison of simulated and experimental results

Table 2 summarizes the simulation and experimental data for each configuration. The differences between the simulation results and the experimental data are attributed to imperfect contact between the switches and the patch antenna. Since an ideal connection was assumed in the simulations, any discrepancies with experimental results can be attributed to imperfect electrical connection. In addition, slight dimensional differences in the placement of the switches on the patch between the simulated and measured results will provide slight changes in the results. Overall, the measured antenna performance matched well with the simulation and is acceptable for antenna applications, indicating the viability of design using simulations of reconfigurable antennas using SMAs.

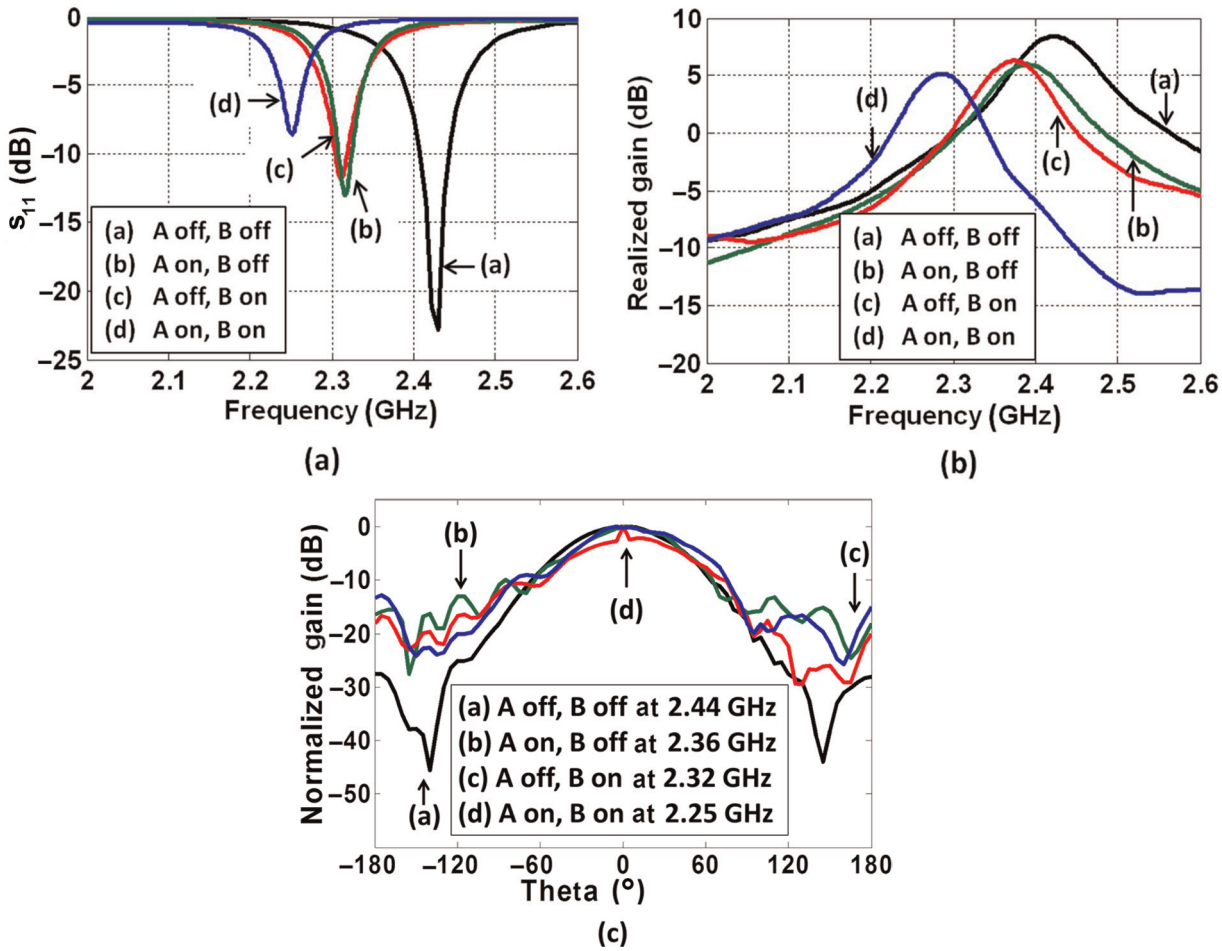

Figure 10. (a) Measured S_{11} and characteristic resonance frequency for each configuration (a–d), (b) measured gain for each configuration, and (c) measured phase for each configuration at the resonant frequencies (a–d).

Table 2. Comparison of simulation results to experimental results of antenna performance for each geometry (a–d).

	RF parameter	Geometry			
		(a) A off, B off	(b) A on, B off	(c) A off, B on	(d) A on, B on
Simulation	Resonant frequency (GHz)	2.44	2.36	2.32	2.27
	Realized gain (dB)	8.11	7.57	7.18	6.78
Measurement	Resonant frequency (GHz)	2.43	2.32	2.31	2.25
	Realized gain (dB)	8.4	6.25	5.96	5.15

RF: radio frequency.

Figure 11 shows a comparison of the simulated and measured results for both switches on and both switches off. From the S_{11} and gain results, there is close agreement between the simulation and measured results, other than the predescribed deviations due to imperfect contact. The radiation pattern also shows strong correlation between data and simulations, with slight deviations due to imperfect contact. The deviations below −20 dB are insignificant to the antenna performance and are therefore disregarded.

Conclusion and future work

The ability to reconfigure the operating frequency of RF antennas is of great potential impact in many applications. SMA switches have been successfully applied in creating a multiband reconfigurable patch antenna structure at radio frequencies. Two switches were built with Ni–Ti that is heated resistively to recover a trained shape through an induced phase change to close an electrical circuit. The removal of the current cools the Ni–Ti, which is subsequently pushed up by a spring steel layer to open the

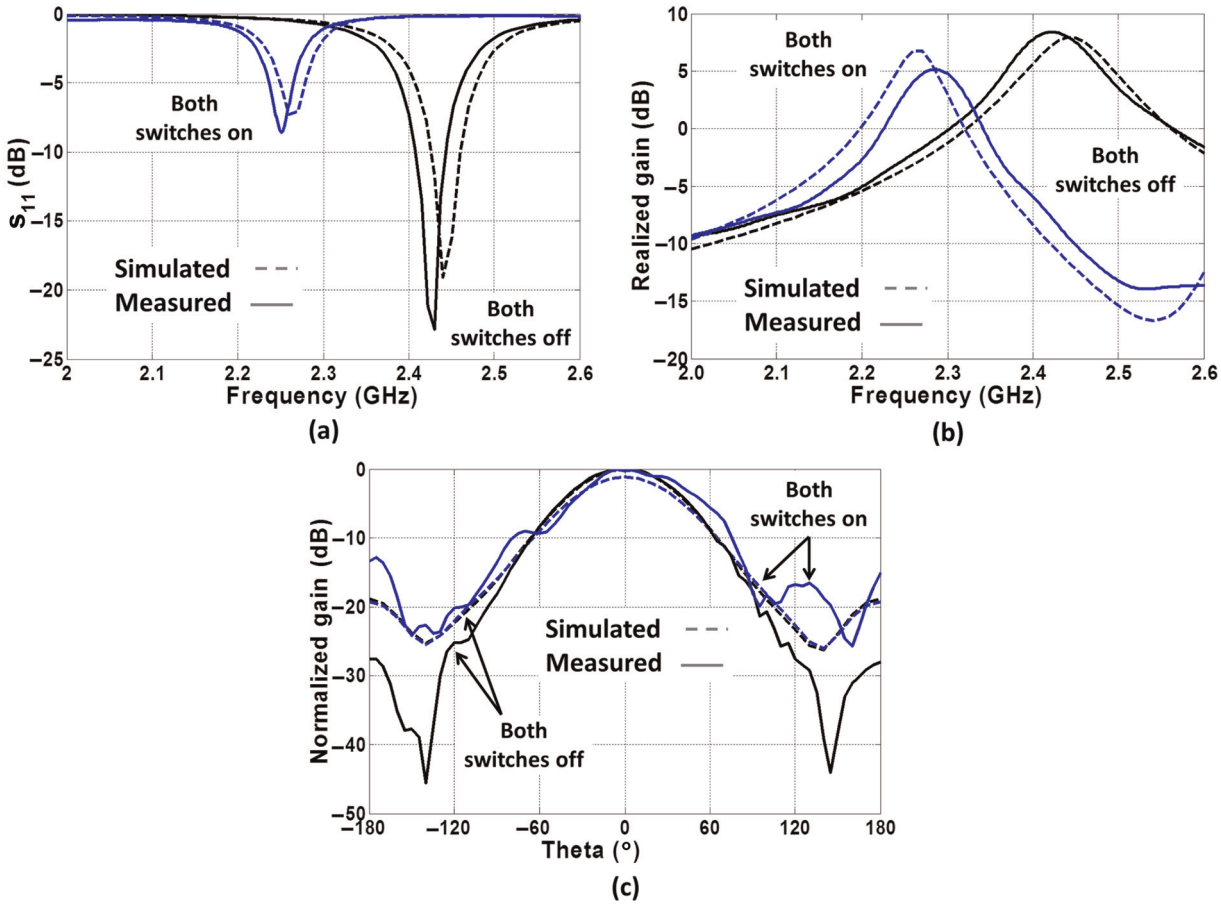

Figure 11. Comparison of measurement and simulated antenna performance for both switches on and both switches off: (a) S_{11}, (b) antenna gain, and (c) radiation pattern.

circuit. Antenna reconfiguration was achieved by controllably activating the switches to an on or off position, creating varying signal pathways within the antenna. The patch antenna exhibited a maximum shift in the resonance frequency from 2.25 to 2.43 GHz. Furthermore, the achieved gain of all four antenna configurations is high (>5 dB) and satisfactory for high-performance wireless communications. The experimental results match well with simulations, indicating the potential for simulated design of future applications and geometries using shape memory actuators. Impedance matching around 50 Ω will be attempted at the SMA coupling interface through alterations to the actuation force of the SMA onto the antenna. The applied coupling force can be altered to affect the impedance of this interface through the switch contact to ensure optimal EM performance. Additionally, further miniaturization of the switches will be investigated for implementation into more complex antenna geometries.

Funding

Financial support for this research was provided by the OSU Institute for Materials Research Interdisciplinary Materials Research Grant and the Smart Vehicle Concepts Center (www.SmartVehicleCenter.org), a National Science Foundation Industry/University Cooperative Research Center.

Acknowledgements

The authors would like to thank John Volakis of the OSU Electro-Science Laboratory for assistance with this work.

References

Anagnostou DE, Zheng G, Chryssomallis MT, et al. (2006) Design, fabrication and measurements of an RF-MEMS-based self-similar reconfigurable antenna. *IEEE Transactions on Antennas and Propagation* 54(2): 422–432.

Arcioni P, Conciauro G, Perregrini L, et al. (2007) Design of MEMS reconfigurable patch antennas via a planar model approach. *IEEE Antennas and Propagation Society International Symposium*, 5191–5194.

Balanis CA (2005) *Antenna Theory: Analysis and Design*. Hoboken, NJ: Wiley-Interscience.

Balanis CA (2008) *Modern Antenna Handbook*. Hoboken, NJ: Wiley-Interscience.

Bernhard JT (2007) *Reconfigurable Antennas*. Synthesis Lectures on Antennas 2(1):1–66.

Bernhard JT, Kiely E and Washington G (2001) A smart mechanically actuated two-layer electromagnetically

coupled microstrip antenna with variable frequency, bandwidth, and antenna gain. *IEEE Transactions on Antennas and Propagation* 49(4): 597–601.

Bhartia P and Bahl IJ (1982) Frequency agile microstrip antennas. *Microwave Journal* 25: 67–70.

Davis JR (2003) *Handbook of Materials for Medical Devices*. OH: ASM International. Materials Park.

Ghosh CK and Parui SK (2010) Design, analysis and optimization of a slotted microstrip patch antenna array at frequency 5.25 GHz for WLAN-SDMA system. *International Journal on Electrical Engineering and Informatics* 2(2): 102–112.

Kai Y and Chengin G (2002) Design and control of novel embedded SMA actuators. *Journal of Electrical and Electronics Engineering* 2(2): 513–520.

Kim JY, Jung CW and Lee B (2011) Reconfigurable beam steering antenna using double loops. *Electronics Letters* 47(7): 430–431.

Lagoudas D (2008) *Shape Memory Alloys*. New York, NY: Springer Science and Business Media, LLC.

Lee KF (1989) Microstrip patch antennas—basic properties and some recent advances. *Journal of Atmospheric and Terrestrial Physics* 51: 811–818.

Liang C and Rogers CA (1997) Design of shape memory alloy actuators. *Journal of Intelligent Material Systems and Structures* 8: 303–313.

Otsuka K and Wayman CM (1999) *Shape Memory Materials*. Cambridge: Cambridge University Press.

Pozar D (1998) *Microwave Engineering*. 2nd edn. New York, NY: John Wiley & Sons.

Targonski SD, Waterhouse RB and Pozar DM (1998) Design of wide-band aperture-stacked patch microstrip antennas. *IEEE Transactions on Antennas and Propagation* 46(9): 1245–1251.

Vinoy KJ and Varadan VK (2001) Design of reconfigurable fractal antennas and RF-MEMS for space-based systems. *Smart Materials and Structures* 10: 1211.

Wolcott PJ, Dapino MJ and Zhang L (2011) Smart switch metamaterials for multiband radio frequency antennas. *Journal of Intelligent Material Systems and Structures* 22(13): 1469–1478.

Yang SS and Luk KM (2006) Design of a wide-band L-probe patch antenna for pattern reconfiguration or diversity applications. *IEEE Transactions on Antennas and Propagation* 54(2): 433–438.

Yashchyshyn Y (2010) Reconfigurable antennas: the state of the art. *International Journal of Electronics and Telecommunications* 56(3): 319–326.